minal $^1J_{Si-H}$ falls by 20 Hz. A lower value of J_{Si-H} is expected in the phosphine-substituted compounds simply because of the basic nature of the phosphines. The bridging J_{Si-H} falls by 27 Hz on going from $MeCp(CO)_2MnHSiHPh_2$ to $MeCp(CO)(PMe_3)MnHSiHPh_2$. Since at least 20 Hz of this change is expected due to the charge redistribution from the phosphine in place of a carbonyl, the decreased coupling due to a decrease in Si-H bonding interaction on going from the dicarbonyl complex to the phosphine complex is no more than 7 Hz. This slight change in the Si-H interaction with the metal from phosphine substitution is consistent with the photoelectron results.

It is evident that the phosphine ligand with its electron density and low π-back-bonding capabilities is not responsible for changing the general nature of the bond interaction in these complexes. The valence photoelectron measurements show that PMe_3 does change the degree of interaction to a small extent, resulting in a slightly stronger Si-H bond interaction with the metal in both phosphine compounds as compared to their dicarbonyl derivatives. The extent of oxidative addition of the Si-H bond to the manganese center in these complexes is strongly favored by electron-withdrawing substituents on the silicon atom and is less improved by substitution of a carbonyl with typical two-electron donor ligands, which increase the electron density at the metal center.

Acknowledgment. We acknowledge support by the donors of Petroleum Research Fund, administered by the American Chemical Society, the U.S. Department of Energy (Division of Chemical Sciences, Office of Basic Energy Sciences, Office of Energy Research) (Grant DE-AC02-80ER 10746), the National Science Foundation (Grant CHE8519560), and the Materials Characterization Program, Department of Chemistry, University of Arizona. We also gratefully acknowledge Professor Ulrich Schubert for supplying samples of $MeCpMn(CO)(PMe_3)HSiCl_3$ and $MeCpMn(CO)(PMe_3)HSiHPh_2$ and for helpful discussions. Swati Chattopadhyay is acknowledged for assistance in assembling the figures.

Contribution from the Inorganic and Structural Chemistry Group (INC-4), Isotope and Nuclear Chemistry Division, Los Alamos National Laboratory, Los Alamos, New Mexico 87545, and Department of Physics, Colorado State University, Fort Collins, Colorado 80523

Studies of Mixed-Valence Linear-Chain Complexes Crystallized at Elevated Pressures. Crystal Structures of $[Pt(en)_2][Pt(en)_2X_2](ClO_4)_4$ (X = Br, I)

Jeffrey B. Weinrach,[†] Scott A. Ekberg,[†] Steven D. Conradson,[†] Basil I. Swanson,*[,†] and H. Dieter Hochheimer[‡]

Received April 26, 1989

The structures of the complexes $[Pt(en)_2][Pt(en)_2Br_2](ClO_4)_4$ (**1**) and $[Pt(en)_2][Pt(en)_2I_2](ClO_4)_4$ (**2**) grown at elevated pressures (7 kbar) have been determined. The bromide is monoclinic with cell dimensions a = 8.307 (2) Å, b = 5.460 (2) Å, c = 8.307 (2) Å, and β = 109.01 (3)°, in space group $P2/m$ with one formula unit of $[Pt(en)_2Br(ClO_4)_2]$ per cell. The iodide is monoclinic with cell dimensions a = 16.908 (2) Å, b = 5.818 (1) Å, c = 7.436 (1) Å, and β = 98.55 (1)°, in space group $C2$ with one formula unit per cell. The structure of the bromide complex has a more symmetrical packing arrangement of the chains with respect to the structure grown under ambient-pressure conditions. The degree of trapped-valence character and the disorder in the position of the bridging bromine ligand are similar to those features of the ambient-pressure structure. The iodide complex has a very similar spatial arrangement compared with its ambient-pressure structure; however the ethylenediamine ligands appear to pack in a more conventional staggered arrangement.

Introduction

Mixed-valence linear-chain complexes have been studied extensively over the last decade. In general, these materials exhibit anisotropic optical and electronic behavior that can be observed with numerous spectroscopic techniques including electronic absorption and resonance Raman spectroscopy.[1-3] Complexes such as those described herein exhibit a Peierls distortion from a delocalized chain of formally Pt(III) metal centers to a trapped-valence chain structure with alternating Pt(II) and Pt(IV) metal centers, resulting in a charge density wave system.[4,5] Associated with these chains are small but noticeable concentrations of local gap states (polarons, bipolarons, excitons, and kinks) that have been characterized by Peierls-Hubbard and other many-body models.[6] These defect states typically have absorption maxima at longer wavelengths with respect to the intervalence charge-transfer band associated with the Pt(II)-Pt(IV) moiety. The defect states can be observed in resonance Raman spectroscopy with vibrational features distinctly different from those in the remainder of the chain.[7,8]

Structural characterization is extremely important in the elucidation of the degree of trapped-valence character along the chains, prediction of the effects of neighboring chains and any counterions on the optical and electronic properties of the material, and the generation and stability of the observed gap states.[9,10] Many reported crystal structures of these linear-chain complexes show disorder due to a stacking fault perpendicular to the chain axis, as shown in Figure 1.[11-13] Also, counterions and waters of hydration often are disordered with respect to their orientation as well as position in the lattice. The structure along the chain usually can be resolved by locating two bridging ligand positions on either side of the centroid position with half-occupancy. However, the possible effects of neighboring chains and counterions

[†] Los Alamos National Laboratory.
[‡] Colorado State University.

(1) Clark, R. J. H.; Kurmoo, M. *J. Chem. Soc., Dalton Trans.* **1981**, 524.
(2) Papavassiliou, G. C.; Layek, D. *Z. Naturforsch.* **1980**, *35B*, 676.
(3) Tanaka, M.; Kurita, S. *J. Phys. C* **1986**, *19*, 3019.
(4) Ueta, M.; Kanzaki, H.; Kobayashi, K.; Toyozawa, Y.; Hanamura, E. *Excitonic Processes in Solids*; Springer Series in Solid-State Sciences, Vol. 60; Springer: Berlin, 1986; Chapter 9.
(5) Onodera, Y. *J. Phys. Soc. Japan* **1987**, *56*, 250.
(6) Baeriswyl, D.; Bishop, A. R. *J. Phys. C* **1988**, *21*, 339.
(7) Conradson, S. D.; Stroud, M. A.; Zietlow, M. H.; Swanson, B. I.; Baeriswyl, D.; Bishop, A. R. *Solid State Commun.* **1988**, *65*, 723.
(8) Conradson, S. D.; Dallinger, R. F.; Swanson, B. I.; Clark, R. J. H.; Croud, V. B. *Chem. Phys. Lett.* **1987**, *135*, 463.
(9) Beauchamp, A. L.; Layek, D.; Theophanides, T. *Acta Crystallogr.* **1982**, *B38*, 1158.
(10) Fanizzi, F. P.; Natile, G.; Lanfranchi, M.; Tiripicchio, A.; Clark, R. J. H.; Kurmoo, M. *J. Chem. Soc., Dalton Trans.* **1986**, 273.
(11) Endres, H.; Keller, H. J.; Martin, R.; Traeger, U.; Novotny, M. *Acta Crystallogr.* **1980**, *B36*, 35.
(12) Beauchamp, A. L.; Layek, D.; Theophanides, T. *Acta Crystallogr.* **1982**, *B38*, 1901.
(13) Cannas, M.; Lucchesini, M. B.; Marongiu, G. *Acta Crystallogr.* **1983**, *C39*, 1514.

0020-1669/90/1329-0981$02.50/0

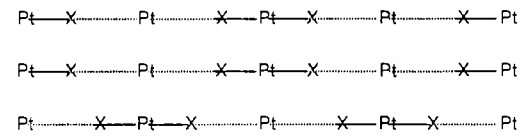

Figure 1. Random stacking arrangement of platinum–halide chains resulting in a halide disorder.

Table I. Crystal Data and Details of Structure Analysis

	$[Pt(en)_2][Pt(en)_2Br_2](ClO_4)_4$	$[Pt(en)_2][Pt(en)_2I_2](ClO_4)_4$
MW	1188.26	1282.26
cryst syst	monoclinic	monoclinic
a/Å	8.307 (2)	16.908 (2)
b/Å	5.460 (2)	5.818 (1)
c/Å	8.307 (2)	7.436 (1)
β/deg	109.01 (3)	98.55 (1)
V/Å	356.31	723.35
space group	$P2/m$	$C2$
Z	1/2	1
ρ_{calcd}/g cm^{-3}	2.77	2.94
$F(000)$	553.1	588.4
μ(Mo Kα)/cm^{-1}	131.4	123.2
cryst size/mm	0.15 × 0.04 × 0.06	0.35 × 0.05 × 0.15
θ range/deg	25	25
no. of total data	2868	2235
no. of unique data	767	706
no. of obsd data	765	705
significane test	$I > 3\sigma$	$I > 3\sigma$
no. of params	58	66
R	0.086	0.055
R_w	0.107	0.081

on the physical properties and the spectroscopic characterization of these quasi-one-dimensional materials are difficult to determine as long as these disorders remain. In an attempt to alleviate the interchain disorder problems, crystals of these linear-chain complexes have been grown at elevated pressure.[14] This crystallization technique should promote order by decreasing the unit cell volume and therefore increasing the interchain interactions.

The crystal structures of the title complexes grown at ambient pressures have been reported previously in the literature.[15,16] The bromide compound (**1**) exists in two distinctly different crystalline forms, both of which show high disorder in the stacking of the chains as well as the orientation of the perchlorate counterion. The iodide structure (**2**), on the other hand, has ordered perchlorate ions with disorder arising from the stacking faults. In both cases, two positions of the bridging halogen, one on either side of the centroid position, were determined.

Experimental Section

High-Pressure Crystallization. Pressure (7 kbar) was generated with a hydraulic pump and intensifier, with an ethanol–methanol mixture being the pressure-transmitting medium. The pressure cell was wrapped with standard 110-V heating tape plugged into a standard Variac transformer. A 3-cm^3 Teflon cell with a quartz window containing a saturated aqueous solution of the title complexes at 40 °C was inserted into the high-pressure cell.[17] An Omega Engineering, Inc., temperature controller (Model No. 6001-P1-T1) with a platinum RTD temperature probe was connected to the Variac transformer. The temperature of the cell was slowly lowered to room temperature over several hours. The cell was then placed in an ice–water bath and cooled over a 24-h period. The conditions for crystal growth were varied in order to optimize the size and quality of the crystals, and this particular rate of cooling was found to give adequate-size crystals for optical and X-ray characterization. After the pressure in the cell was released, the Teflon cell was removed and crystals of the platinum complexes were removed from the cell and harvested.

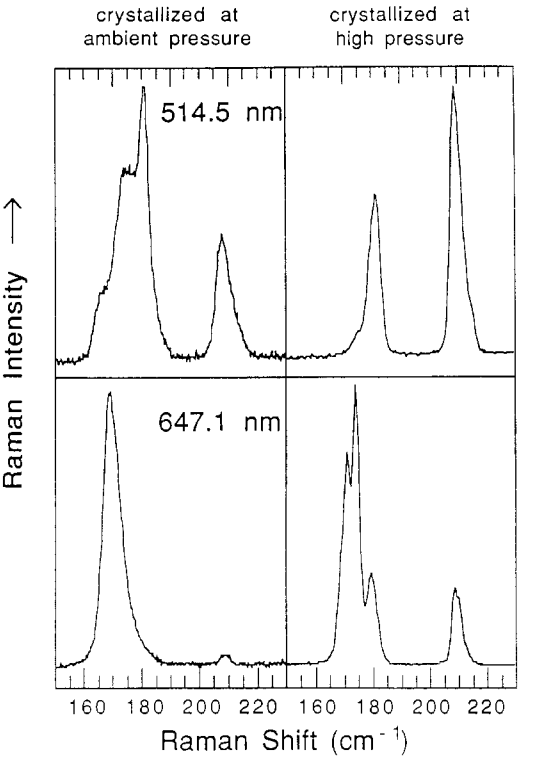

Figure 2. Comparison of the Raman spectra of the bromide complex crystallized at ambient pressure and high pressure at 514.5 and 647.1 nm.

Crystallographic and Raman Studies. Intensity data were collected on a Nonius CAD4 diffractometer to a θ maximum of 25° (graphite-monochromated Mo Kα radiation) by using the ω–2θ scan mode. Empirical absorption corrections and decay corrections were applied after data collection. Crystal data are specified in Table I. Twenty-five reflections were used for unit cell determination. All computations were carried out by using locally written software. Optical microscopy was carried out with a Zeiss polarizing microscope equipped with a Bertrand lens. Raman spectra of oriented single crystals were obtained at several different wavelengths with the use of Kr and Ar ion lasers (Spectra Physics Model 171). The crystals were mounted in a cell that had been pressurized to 13 atm with He gas, and this cell was then fixed to the cold end of a Displex cryostat. The temperature was nominally 10 K, and the laser power was maintained at 5 mW or less to avoid sample heating. The data were obtained by using a JY U1000 double monochromator equipped with an RCA 31034 photomultiplier tube.

Solution to and Refinement of the Structure of $[Pt(en)_2][Pt(en)_2Br_2](ClO_4)_4$. The initial cell obtained from precession photographs suggested a C-centered orthorhombic cell. Intensity measurements, however, confirmed the crystal system to be monoclinic, with the unique axis being the c axis.[18] The cell was therefore reduced to the corresponding primitive cell. Three possible space groups, $P2$, Pm, and $P2/m$, were consistent with the systematic absences. $P2$ was initially chosen due to the molecular geometry. A Patterson function was interpreted to give a platinum atom peak that was chosen to be an origin. A peak due to the bromine atoms was found at (0, 0, 0.5) All other atomic positions were located via difference Fourier synthesis. The carbon atom positions were located at $z = 0$ initially, implying a planar ethylenediamine ligand. Anisotropic refinement revealed a large thermal parameter along the c direction for both the carbon atoms and the bridging bromine ligand. At this juncture, mirror symmetry was imposed (space group $P2/m$) and new atomic positions for these atoms were located on either side of the mirror plane with half-occupancies. Once these positions were located, the mirror plane was lifted and the z coordinates were fixed. Four possible ethylenediamine orientations were considered with the lower symmetry. All four orientations were able to be refined with the same R factor. The F_o map for a particular orientation did not show the presence of the other two carbon positions. It was at this juncture that $P2$ was ruled out due to the apparent singularity in the least-squares refinement of the structure.

(14) Brown, G. Personal communications.
(15) Matsumoto, N.; Yamashita, M.; Kida, S.; Ueda, I. *Acta Crystallogr.* **1979**, *B35*, 1458.
(16) Keller, H. J.; Müller, B.; Ledezma, G.; Martin, R. *Acta Crystallogr.* **1985**, *C41*, 16.
(17) Extreme care should be taken in the handling of aqueous perchlorate solutions. See, for example, the Merck Index.
(18) The supplementary material accompanying the article contains the R_{av} factors for the monoclinic and orthorhombic crystal systems.
(19) Donohoe, R.; Worl, L.; Swanson, B. I. Unpublished results.

Table II. Bond Lengths (Å) and Angles (deg) for **1** and **2**

	1		2
Pt-Br	2.442 (7)	Pt-I	2.733
	3.018 (7)		3.085
Pt-N	2.067 (22)	Pt-N	2.044 (15)
	2.104 (29)		2.063 (15)
N-Pt-N	96.15 (1.1)	N-Pt-N	96.95 (.58)
	83.85 (1.1)		82.96 (.60)
Cl-Cl	1.501 (26)	Cl-O	1.321 (33)
Cl-O	1.469 (28)		1.505 (43)
	1.469 (30)		1.461 (29)
	1.467 (28)		1.454 (21)
	1.467 (29)	O-Cl-O	109.31 (1.9)
O-Cl-O	103.83 (2.35)		117.51 (2.2)
	103.99 (2.26)		121.05 (1.9)
N-C	1.480 (55)		99.30 (2.3)
	1.481 (55)		98.78 (2.0)
	1.543 (55)		107.05 (1.6)
	1.544 (55)	N-C	1.524 (28)
C-C	1.375 (67)		1.464 (33)
		C-C	1.388 (36)

The structure was then resolved in $P2/m$ without the mathematical problems associated with the noncentrosymmetric structure. More atoms were able to be refined with anisotropic temperature factors without fixing the positional parameters. A unique orientation of the ethylenediamine ligand structure was not attainable in this space group, however.

Two chlorine positions with equal intensity were located on either side of $y = 0$ with an interatomic distance of 1.5 Å. These positions were subsequently refined with half-occupancies. Two oxygen atom peaks were located at $y = 0$, bisecting the two chlorine positions (see Figure 2). On the basis of the size of the isotropic thermal parameters for these oxygen positions, full-occupancy rather than half-occupancy was used in further refinements. The remaining oxygen positions were not able to be located directly by difference Fourier synthesis.

Solution to and Refinement of the Structure of $[Pt(en)_2][Pt(en)_2I_2](ClO_4)_4$. Systematic absences showed the cell to be *C*-centered with the *b* axis unique. Three possible space groups ($C2$, Cm, and $C2/m$) were considered. On the basis of the molecular geometry, the space group $C2$ was used in the structural refinements. A Patterson solution was used to locate the platinum position to be at an origin. The bridging iodine ligand was located at (0, 0.5, 0). All other atoms were located via difference Fourier synthesis. One of the two carbon atom positions of the ethylenediamine ligand appeared on either side of $z = 0$. However, during the refinement cycles of the carbon positions, the one position with a slightly positive z coordinate refines with full-occupancy with a more reasonable isotropic thermal parameter. The atomic position with a slightly negative z coordinate refines across $z = 0$ to the other position. The perchlorate counterion refines in one orientation with the oxygen atoms ordered. Mirror symmetry was imposed to find the position of the bridging iodide ligand off the centroid position. Once its position was refined with the mirror plane, it was lifted and the positional and thermal coordinates were fixed.

Results and Discussion

$[Pt(en)_2][Pt(en)_2Br_2](ClO_4)_4$. Important bond lengths and angles for **1** are given in Table II, and final fractional atomic coordinates and thermal parameters are given in Table III.

The structure of the Pt-Br compound grown at high pressure is somewhat analogous to the monoclinic form previously reported, except for a slight but relevant shift in the chain stacking to a more symmetric lattice. The crystal structure of the bromide complex (monoclinic phase) previously reported shows the *a* and *c* axes being inequivalent as well as the perchlorate counterions occupying asymmetric positions in close proximity to the diagonal axis. The high-pressure structure shows the *a* and *c* axes to be equivalent with the perchlorate counterions occupying symmetric positions on either side of the diagonal axis with half-occupancies.

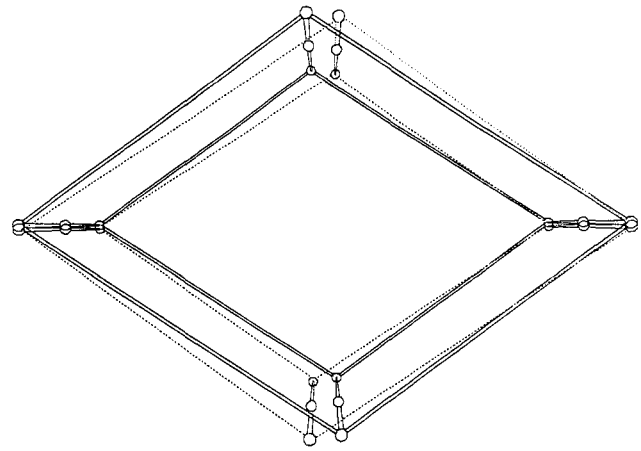

Figure 3. Superposition of the ambient-pressure bromide structure on its mirror image, showing the spatial arrangement of the platinum atoms.

It is not clear, at present, why PtBr grown at high pressure crystallizes in a more symmetric packing arrangement of the chains. However, the reduced molecular volume at high static pressure will, most certainly, give rise to stronger interchain, interionic, and hydrogen-bonding interactions, which should result in more efficient packing.

In order to demonstrate that this apparent phase change was not due to microscopic twinning with respect to the chain axis, optical microscopy was used to show the crystals to have a high degree of birefringence. The isogyres representing the orientation of the polarizer and analyzer appeared clearly under cross-polarization conditions, thereby ruling out a microscopic twin. Another indication that the observed structure is not a result of twinning is the relatively small size of the platinum thermal ellipsoids. By occupying an origin position in the unit cell, the platinum atom would be occupying two distinct sites in a twinned crystal. This would lead to a large thermal parameter for the platinum atom averaged over the two sites (see Figure 3).

Raman spectroscopy shows sharper bandwidths for the peaks associated with the Pt-Br stretching mode as compared with the original material. This band narrowing could result from a higher degree of order in the high-pressure crystals (see Figure 2); intimate twinning of the crystals would have resulted in band broadening rather than band narrowing. Alternatively, this band narrowing could simply be a result of less inhomogeneous broadening by virtue of a lower concentration of defect states. In this regard, it is also worth noting that the intensities of the component bands of ν_1 that have been attributed to gap states and the normal chain mode[8] relative to the putative N-Pt-N deformation at 212 cm^{-1} are lower in the crystals grown at high pressure than for those grown under ambient conditions. This effect is evident in the comparison of the Raman spectra obtained for the two different crystal types by using red (647.1 nm) versus blue (514.5 nm) excitation. Recent spectral studies[19] have shown that the 212-cm^{-1} feature corresponds to a hole-bipolaron defect state that is selectively enhanced with excitation well to the blue of the band edge (ca. 850 nm). In general, the large differences in relative intensities of the component bands in the two different crystal types result from differing concentrations of local defect states.

The degree of trapped valency in the bromide structure appears to be equivalent to that of the ambient-pressure structure, as

Table III. Fractional Coordinates and Thermal Parameters for **1**

atom	*x*	*y*	*z*	*B*, Å²	atom	*x*	*y*	*z*	*B*, Å²
Pt(1)	0.0000 (0)	0.0000 (0)	0.0000 (0)	1.79[a]	Cl(1)	0.377 (2)	0.500 (0)	0.222 (3)	4.8[a]
Cl(2)	0.221 (3)	0.500 (0)	0.377 (2)	4.6[a]	N(1)	0.266 (4)	0.000 (0)	0.944 (4)	4.3[a]
N(2)	0.059 (3)	0.000 (0)	0.738 (3)	3.2[a]	O(1)	0.261 (4)	0.288 (4)	0.262 (4)	9.7[a]
C(1)	0.339 (7)	0.048 (0)	0.750 (6)	4.3*a*	C(2)	0.243 (6)	0.054 (9)	0.660 (5)	4.3[a]
Br(1)	0.0000 (0)	0.5528 (12)	0.0000 (0)	3.62 (13)					

[a] $(u11 + u22 + u33)/3$; anisotropic thermal parameters are published as supplementary data.

Table IV. Fractional Coordinates and Thermal Parameters for **2**

atom	*x*	*y*	*z*	*B*, Å^2	atom	*x*	*y*	*z*	*B*, Å^2
Pt(1)	0.0000 (0)	0.0000 (0)	0.0000 (0)	1.317[a]	Cl(1)	−0.140 (0)	0.490 (3)	0.527 (1)	3.2[a]
O(1)	−0.096 (2)	0.303 (7)	0.537 (4)	4.0[a]	O(2)	−0.087 (2)	0.699 (7)	0.537 (4)	5.9[a]
O(3)	−0.183 (1)	0.540 (9)	0.680 (4)	6.4[a]	O(4)	−0.194 (2)	0.548 (5)	0.362 (3)	6.9[a]
I(1)	0.0000 (0)	0.5303 (0)	0.0000 (0)	2.184 (0)	I(2)	0.0000 (0)	0.4697 (0)	0.0000 (0)	2.184 (0)
N(1)	0.056 (1)	0.006 (9)	−0.225 (2)	1.8 (3)	N(2)	0.116 (1)	0.014 (9)	0.135 (2)	2.1 (3)
C(1)	0.145 (2)	−0.039 (5)	−0.174 (4)	2.6 (6)	C(2)	0.171 (2)	−0.057 (4)	0.011 (4)	2.1 (5)

[a] $(u11 + u22 + u33)/3$; anisotropic thermal parameters are published as supplementary data.

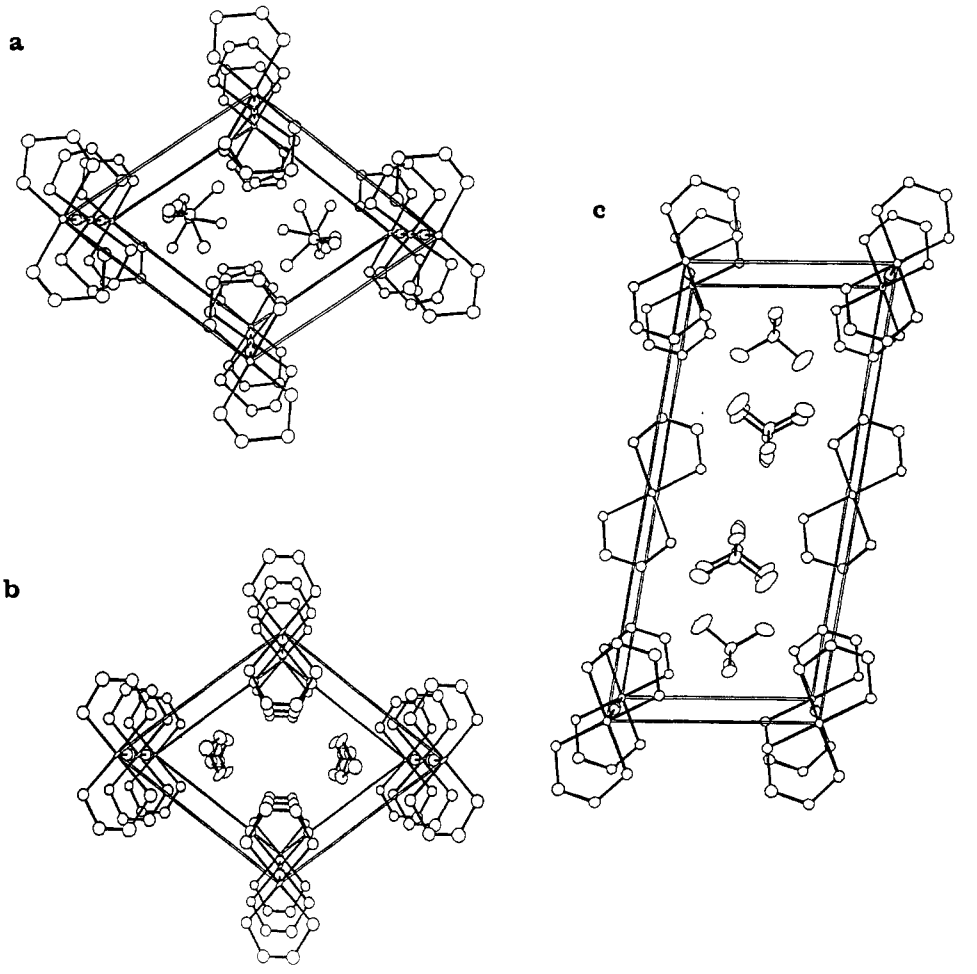

Figure 4. (a) Packing diagram of the ambient-pressure bromide structure. (b) Packing diagram of the high-pressure bromide structure. (c) Packing diagram of the high-pressure iodide structure.

indicated by the Pt–Br bond lengths. This is also evident by the wavenumber and intensity of the Raman band attributed to the Pt–Br stretch, which is essentially the same as that of the other PtBr structures.

$[Pt(en)_2][Pt(en)_2I_2](ClO_4)_4$. The important bond lengths and angles for **2** are shown in Table II, and the atomic coordinates and thermal parameters are listed in Table IV.

Unlike the bromide structure which crystallized in a more symmetrical lattice, the iodide structure does not change its intermolecular packing appreciably under high-pressure conditions. However, it should be noted that the ambient-pressure structure of the iodide complex is much more asymmetric in its chain packing than the bromide analogue. Figure 4 shows the three packing diagrams: (a) the ambient-pressure bromide structure, (b) the high-pressure bromide structure, and (c) the iodide structure. The high-pressure bromide structure packs in a diamond-shaped lattice with all the platinum atoms aligned along the same lattice planes. The iodide structure, on the other hand, packs in a rectangular arrangement with alternating platinum atoms and iodine atoms along the lattice planes. This structure resembles more closely the orthorhombic phase of the bromide complex than the monoclinic phase. A more symmetric lattice should be attainable but under more drastic growing conditions.

Conclusion

Under high-pressure crystallization conditions, the bromide complex crystallizes in a more symmetrical lattice. In order to compensate for the change in the packing arrangement, the perchlorate counterions occupy two sites on either side of the diagonal axis. The iodide structure, which is quite different from the monoclinic bromide structure in its packing arrangement, did not undergo a major structural distortion under high-pressure crystallization. There were, however, slight modifications in the orientation of the ethylenediamine ligands in these structures.

The extent to which counterions and neighboring chains affect the overall stacking of the chains is readily seen in the two structures reported herein. When a bridging bromide is replaced with an iodide ion and the Pt–Pt distance is increased by only 0.4 Å, the overall packing arrangement of the chain structure changes tremendously. Hydrogen bonding of the perchlorate counterions seems important in determining the overall structure of these complexes. Using pressure as a tool in crystallization should help to elucidate the role that these counterions play in the stability of these materials as well as the interactions between neighboring

chains. It is also our intention to perform X-ray crystallography measurements at high static pressure to study the pressure effects on the crystal lattice in these materials and to assess the relaxation effects that take place when pressure is released.

Acknowledgment. We thank Robert R. Ryan, Carol J. Burns, and Don T. Cromer for helpful discussions. This work was performed under the auspices of the U.S. Department of Energy with support from the Office of Basic Energy Sciences, Materials Science Division, and the Center for Materials Sciences of Los Alamos National Laboratory.

Supplementary Material Available: Tables of intensity data for determining the crystal system of **1** and anisotropic thermal parameters for **1** and **2** (2 pages); tables listing structure factors for **1** and **2** (3 pages). Ordering information is given on any current masthead page.

Contribution from the Departments of Chemistry and Biophysics, University of Rochester, Rochester, New York 14642, and Squibb Institute for Medical Research, P.O. Box 191, New Brunswick, New Jersey 08903-0191

Nuclear Magnetic Relaxation in Aqueous Solutions of the Gd(HEDTA) Complex

Griselda Hernandez,[†] Harry G. Brittain,[§] Michael F. Tweedle,[§] and Robert G. Bryant*[,‡]

Received April 5, 1989

The luminescence decay times and rate constants of terbium complexed with HEDTA (*N*-(2-hydroxyethyl)ethylenediaminetriacetic acid) are obtained at pH values ranging from pH 1.5 to 12 and used to determine the number of water molecules bound at the inner coordinate sphere of the lanthanide complex. The proton nuclear magnetic relaxation rate, $1/T_1$, is reported as a function of pH for gadolinium complexed with HEDTA over a range of magnetic field strengths corresponding to proton Larmor frequencies between 0.01 MHz and 30 MHz. The data analysis is largely based on the Solomon, Bloembergen, and Morgan equations after the outer-sphere contribution is taken into account. The number of water molecules in the first coordination sphere was measured by using fluorescence lifetime methods and the assumption that the result is the same for the lanthanide complex of gadolinium and terbium. The parameters obtained from the analysis are consistent with other estimates of interatomic distances and rotational correlation times. Further, the data show that the dimerization of the complex at high pH does not compromise the relaxation efficiency of the metal center, but it increases approximately by a factor of 2.

Control of magnetic relaxation holds promise for important applications in medical imaging and diagnosis. Further, if the relaxation is coupled to specific chemistry, the control of relaxation may provide a remote reporter of localized organ function using conventional magnetic imaging methods. Of the several classes of magnetic relaxation agents,[1-3] paramagnetic metal complexes provide excellent relaxation efficiency as well as a very rich chemistry that permits considerable flexibility in the control of reagent delivery in vivo. Ions with long electron spin relaxation times are most efficient affectors of nuclear spin relaxation. For paramagnetic centers with short electron relaxation times, the dominant contribution to the correlation time for the electron–nuclear coupling may be the electron relaxation itself. If this relaxation time is shorter than rotational or exchange correlation times, the efficiency of the paramagnetic center for nuclear relaxation is limited. For very short electron spin relaxation times, the dominant effect may be a large induced chemical shift rather than relaxation.[4-6] Thus, attention has focused on the atoms with S state electronic structures such as manganese(II) and gadolinium(III). Many of the clinically interesting complexes are based on chelating agents comprised largely of carboxylate groups such as EDTA or DTPA.[7] Though these complex ions appear to be very simple, their chemistry may be complicated by structural and electronic changes as a function of the complex ion dynamics or structure, which may be altered by pH or the apparent viscosity of the medium. In the present report we focus on the pH dependence of the water proton spin relaxation in aqueous solutions of Gd(HEDTA), which was chosen because aggregation of this complex has been demonstrated at alkaline pH values and thus provides a convenient approach to quantitative assessment of the relaxation effects associated with bringing two paramagnetic centers very close together.

Experimental Section

Nuclear magnetic relaxation measurements were made on a field-cycling spectrometer that switches magnetic field strengths in real time from values limited by Earth's magnetic field to a proton Larmor frequency of 42 MHz using a field controller and passing stage built at the IBM Watson Laboratories in the laboratory of Dr. Seymour Koenig.[8-11] Three Sorensen SRL-60-35 power supplies operated in parallel provide the main current source, supplemented by a capacitor bank and a secondary power supply for rapid field switches. The system employs a copper-wound solenoid bathed in liquid nitrogen to handle the heat dissipation. The probe is a single saddle coil inductor mounted at the end of a rigid coaxial line that forms a component of the resonant probe circuit, the remaining capacitive elements of which reside outside the magnet and cryostat. A simple parallel tuned circuit is used that is matched with a single series capacitor.

The radio frequency spectrometer derives the resonance frequency from a crystal oscillator at 21 or 7.25 MHz, which is amplified after a Vari-L rf SS-30 rf gate by an ENI 10-W broad-band amplifier. The receiver is protected in the usual way with series-crossed diodes on the transmitter side and crossed diodes to ground at the input to the Meiteq preamplifier located one-fourth of a wavelength from the transmitter insertion. The preamplifier is followed by an Avantek 502-515 series cascade that operates into a Merrimack doubly balanced mixer where the reference is typically set 300 kHz from the resonance frequency. The resulting demodulated signal at 300 kHz is then detected with an absolute value detector to yield an audio signal that is amplified and filtered by using a homemade system.

In a typical experiment the spins are first brought to a proton resonance frequency of 30 MHz and polarized there for a period of $5T_1$. The field is then switched to a value of interest for a variable time, τ, after

* To whom correspondence should be addressed at the Biophysics Department, University of Rochester Medical Center, Rochester, NY 14642.
† Department of Chemistry, University of Rochester.
‡ Departments of Chemistry and Biophysics, University of Rochester.
§ Squibb Institute for Medical Research.

(1) Brasch, R. C. *Radiology* **1983**, *147*, 781.
(2) Wolf, G. L.; Joseph, P. M.; Goldstein, E. J. *Am. J. Radiol.* **1986**, *147*, 367.
(3) Koenig, S. H.; et al. *Invest. Radiol.* **1986**, *21*, 697.
(4) Dwek, R. A. *Nuclear Magnetic Resonance in Biochemistry, Applications to Enzyme Systems*; Clarendon: Oxford, England, 1973.
(5) La Mar, G. N., Horrocks, W. D., Holm, R. G., Eds. *NMR of Paramagnetic Molecules*; Academic: New York, 1973.
(6) Bertini, I.; Luchinat, C. *NMR of Paramagnetic Molecules in Biological Systems*; Benjamin/Cummings: Menlo Park, CA, 1986.
(7) Lauffer, R. B. *Chem. Rev.* **1987**, *87*, 901.
(8) Redfield, A. G.; Fite, W., II; Blerch, H. E. *Rev. Sci. Instrum.* **1968**, *39*, 710.
(9) Hallenga, K.; Koenig, S. H. *Biochemistry* **1976**, *15*, 4255.
(10) Brown, R. D.; Brewer, C. F.; Koenig, S. H. *Biochemistry* **1977**, *16*, 3883.
(11) Fukushima, E.; Roeder, S. B. W. *Experimental Pulse NMR, A Nuts and Bolts Approach*; Addison-Wesely Publishing Co., Inc.: Reading, MA, 1981.

0020-1669/90/1329-0985$02.50/0